RESEARCH ARTICLE

ADVANCED PHYSICS RESEARCH Open Access

www.advphysicsres.com

Parametric Excitation and Instabilities of Spin Waves Driven by Surface Acoustic Waves

Moritz Geilen, Roman Verba, Abbass Hamadeh, Alexandra Nicoloiu, Daniele Narducci, Adrian Dinescu, Milan Ender, Morteza Mohseni, Florin Ciubotaru, Mathias Weiler, Alexandru Müller, Burkard Hillebrands, Christoph Adelmann, and Philipp Pirro**

The parametric excitation of spin waves by coherent surface acoustic waves in metallic magnetic thin film structures is demonstrated experimentally using Brillouin light scattering spectroscopy. Complementary micromagnetic simulations and analytical modeling reveal that, depending on the experimental conditions, the spin-wave instabilities originate from different phonon-magnon and magnon-magnon scattering processes. This opens novel ways to create micro-scaled nonlinear magnonic systems for logic and data processing that profit from the efficient excitation of phonons using piezoelectricity.

1. Introduction

Magnetoelasticity, the interaction between magnetism and elastic strain, is a promising mechanism for compact and energy-efficient spintronic devices. In particular, the influence of elastic strain on spin waves, the fundamental excitations in a magnetic solid, is a crucial topic. Many studies have shown that a magnetic field is generated by static strain due to the Villari effect, which can be used to manipulate the ferromagnetic resonance or the propagation of spin waves.[1–4] The interaction between dynamic strain, in the form of bulk acoustic waves (BAWs), and spin waves, and accordingly the formation of hybrid magneto-elastic waves has been studied extensively already in the 1950s and 1960s. As theoretically suggested by Kittel,[5] the excitation of BAWs by spin waves[6] and conversely the excitation of spin waves by BAWs has been demonstrated.[7] In the linear regime of magneto-elastic coupling, it is proven that the frequency and momentum of the initial wave is transferred during the excitation. In the nonlinear regime, the parametric excitation of BAWs has been shown in high-power ferromagnetic resonance experiments.[8] The parametric interaction of spin waves by BAWs, on the other hand, has been theoretically described[9] and indirectly demonstrated by Morgenthaler.[10] Parametric pumping of magnons by BAWs has been detected by inductive microantennas[11] and by the inverse spin Hall effect.[12,13]

In recent years, however, magneto-elastic[14–18] and magneto-rotational[19] coupling of surface acoustic waves (SAWs) with spin waves has attracted significant interest. Since SAWs are localized on the surface of a substrate, they are particularly sensitive to changes in surface conditions caused by (magnetic) films, opening up new possibilities for hybrid systems and devices.[20,21] This, together with efficient and narrow-band excitation of SAWs on piezoelectric substrates and their low propagation losses, has led to their commercial success in RF filters and sensors.[22,23] The excitation of spin waves by SAWs and the associated effects on SAWs have been demonstrated in various material systems, magnetic configurations and by different experimental techniques.[24–32] SAW to SW conversion represents a realistic path toward energy efficient, voltage-controlled spin-wave excitation, which is a key requirement for the application of magnonic circuits,[33–35] as opposed to standard direct SW excitation by microwave transducers, suffering from high Ohmic losses at micro- and nanoscale. However, previous works are all in the linear excitation regime. Although theoretically predicted,[36,37] nonlinear parametric interaction between spin waves and SAWs has rarely been investigated.[38,39] Such nonlinear interactions would be interesting for neuronal networks where non-linear processes with

M. Geilen, A. Hamadeh, M. Ender, M. Mohseni, M. Weiler, B. Hillebrands, P. Pirro
Fachbereich Physik and Landesforschungszentrum OPTIMAS
Rheinland-Pfälzische Technische Universität Kaiserslautern-Landau
67663 Kaiserslautern, Germany
E-mail: hamadeh@rptu.de; ppirro@rptu.de

R. Verba
Institute of Magnetism
Kyiv 03142, Ukraine

A. Nicoloiu, A. Dinescu, A. Müller
National Institute for Research and Development in Microtechnologies
Bucharest R-07719, Romania

D. Narducci, F. Ciubotaru, C. Adelmann
imec
Leuven B-3001, Belgium

D. Narducci
Departement Materiaalkunde
KU Leuven
3001 Leuven, Belgium

The ORCID identification number(s) for the author(s) of this article can be found under https://doi.org/10.1002/apxr.202400086

DOI: 10.1002/apxr.202400086

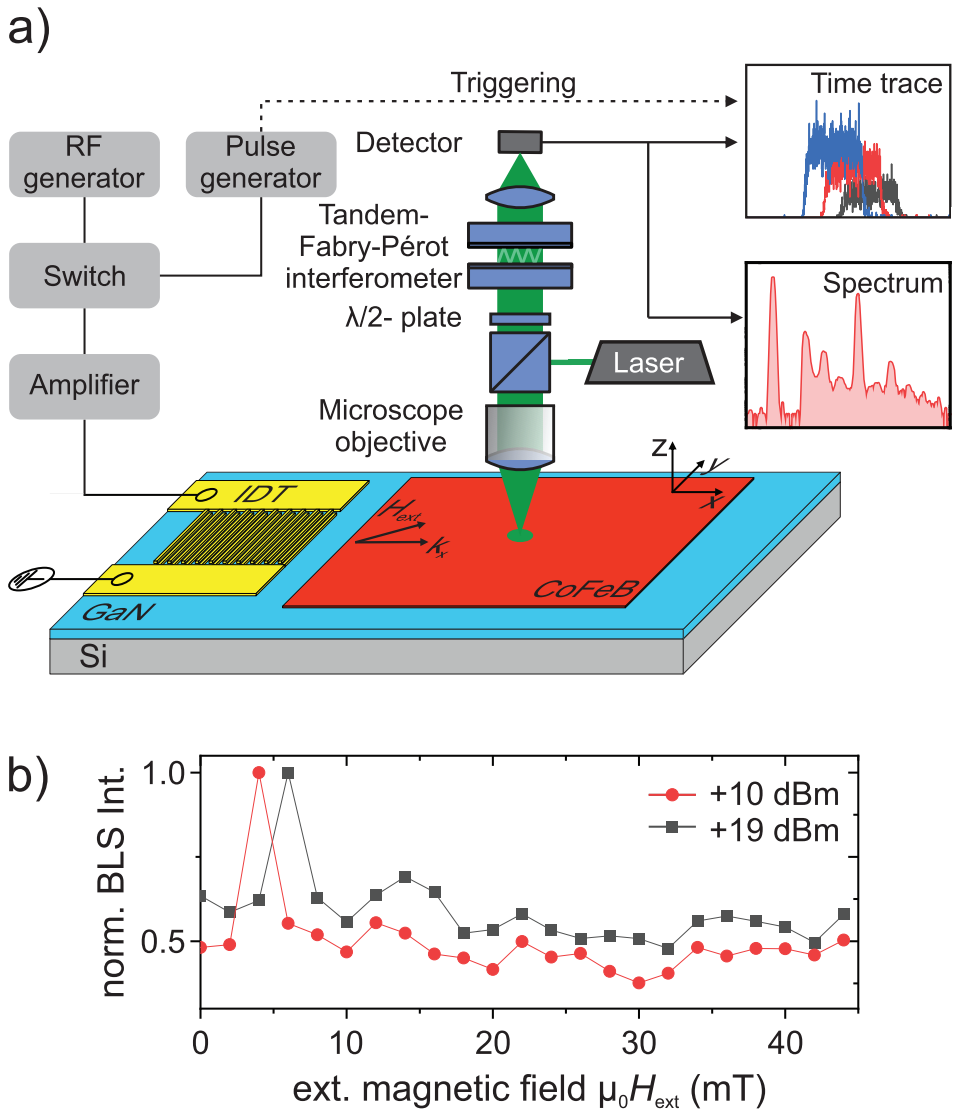

Figure 1. a) Schematic illustration of the experimental setup. SAWs are excited by the IDT and propagate toward a 350 × 350 μm^2 square pad made from a $Co_{40}Fe_{40}B_{20}$ thin film with thickness h_{CoFeB} = 18 nm. b) Normalized BLS intensity at the frequency of the fundamental mode f_0 = 6.3 GHz as a function of the applied magnetic field for the linear and non-linear case. The maxima correspond to the resonant excitation of spin waves by the SAWs. The change in the resonance field with power is caused by the nonlinear shift.

concomitant threshold are a crucial feature,[40] or for multitone microwave emission,[41] and it is an open question if SAW-SW interaction could be strong enough to reach the nonlinear regime of SW dynamics.

2. Experimental Setup and Methodology

In this article, we study spin-wave instabilities, in particular the parametric excitation of spin waves by coherent SAWs in a thin metallic ferromagnetic film of CoFeB. Depending on the bias magnetic field, the magnetization dynamics is directly, or alternatively, parametrically driven by the magneto-elastic field generated by SAWs. Micro-focused Brillouin light scattering spectroscopy (μBLS, see **Figure 1**a) is used to study the different spin-wave modes in a frequency-resolved manner and to reveal the threshold behavior of the instability processes. Analytical modeling combined with full micromagnetic simulations is used to reveal the complex excitation schemes of the different instability processes by identifying the involved mechanisms and magnon modes. Depending on the experimental conditions, a four-magnon instability of the magnon mode, linearly driven by the phonon, is observed as well as a direct first-order parametric phonon-to-magnon instability, which is enhanced by three-magnon splitting of the non-resonantly driven magnon, and even three-wave magnon and magnon-phonon confluence processes.

3. Results and Discussion

In our experiment, an interdigital transducer (IDT) is used to generate surface acoustic waves with a frequency f_{SAW} = 6.31 GHz

and a wave vector $|k_{SAW}| = 9.2$ rad μm^{-1} in a 1.3 μm thick GaN layer on a silicon substrate. Details on the SAW excitation and propagation can be found in ref. [42]. The spin waves are excited in a 350 × 350 μm^2 rectangular pad made from a $Co_{40}Fe_{40}B_{20}$ thin film[43] with thickness $h_{CoFeB} = 18$ nm and are measured by μBLS.[29,44,45] We have chosen CoFeB as a magnetic material since it provides a good compromise between magneto-elastic coupling and spin-wave damping. For an in-plane magnetized film, the excited Rayleigh waves create an effective magnetoelastic field $\mu_0 H_{mel} = -(2B_1 S_{xx} M_x / M_s^2 \mathbf{e_x} + B_2 S_{xz} M_x / M_s^2 \mathbf{e_z})$, where S_{ij} is the SAW strain and B_1 and B_2 are the magneto-elastic coupling constants of the ferromagnet. In this work, we have set $B_1 = B_2 = -8.8$ MJ/m^3 in both the numerical simulations and the analytical model, which is a natural assumption for a polycrystalline CoFeB film. Thus, any anisotropy in the magneto-elasticity is ignored in our study. To ensure that the torque acting on the static magnetization due to magneto-elastic interaction is close to its maximum, the external static magnetic bias field is applied in-plane at an angle of $\varphi = 45°$ with respect to the propagation direction of the SAWs, as shown in Figure 1a (note, that for a SAW $|S_{xz}| \ll |S_{xx}|$ near the surface).

3.1. Resonant Spin-Wave Excitation

Recently, we have demonstrated the excitation of spin waves by SAWs in the linear excitation regime.[29] A strong increase in the spin-wave intensity was observed at the resonance field, where both the frequency and the wave vector of the SAWs are transferred to the spin wave (f_{SAW}, k_{SAW}) = (f_0, k_0). This increase can also be observed in the case presented in this article as shown in Figure 1b. For low excitation powers a resonant spin-wave excitation is observed at a magnetic bias field of 4mT. For higher excitation powers the spin-wave dispersion relation is shifted to lower frequencies, due to the nonlinear shift.[46]

First, the case of approximately resonant spin-wave excitation by the magneto-elastic field beyond the linear regime is studied. The magnetic field is kept constant at $\mu_0 H_{ext} = 6$mT – as follows from Figure 1b, this selection ensures the resonance conditions for energy and momentum conservation are met at larger power, i.e., in the nonlinear regime. The BLS spectrum for magnons is measured as a function of the RF power P applied to the IDT, which is varied between 0dBm and + 30 dBm (see **Figure 2a**). For low power levels, only the directly excited mode f_0 is present. (Please note that the signal at f_0 also includes a residual signal from SAW, which cannot be completely suppressed.[29]) If the power is increased, the appearance of two additional secondary modes $f_1 = 5.7$ GHz and $f_2 = 6.9$ GHz can be observed close to f_0. These two modes satisfy the energy conservation law $2f_0 = f_1 + f_2$ and, thus, can be attributed to a parametric instability of the second-order.[47] For $P \gtrsim 22$dBm (see Figure 2b, blue line), spin waves are excited throughout a broad range of the spin-wave band. These spin waves are caused by further, higher-order scattering channels. This region, which is referred to as the supercritical regime,[47,48] will not be considered further. Instead, we will restrict ourselves to the region close to the threshold where only a single instability process occurs.

A characteristic property of nonlinear instability processes is the existence of a threshold in the initial spin-wave mode's amplitude. This threshold is determined by the minimum of the ratio between the effective relaxation frequency and the coupling strength between the involved magnon modes.[46,47,49,50] The BLS intensity around the three involved modes is extracted, in a way that the secondary modes lay within the spectral range even though their frequencies are changing due to non-linear effects (Supporting Information). The power dependency of the three involved modes is presented in Figure 2c. Once the threshold (P^{th} = + 13 dBm) is overcome a sufficient energy flow into the secondary modes appears and an abrupt increase of the intensity of f_1 and f_2 is visible. The deviation of the mode f_0 from the linear power law is mainly due to nonlinear processes in the SAW excitation. It should be mentioned that SAWs themselves can also exhibit nonlinear processes at sufficiently high amplitudes.[51,52] These would also lead to a deviation from the linear behavior that is usually caused by the generation of higher harmonics, which, however, have not been observed in our experiment.

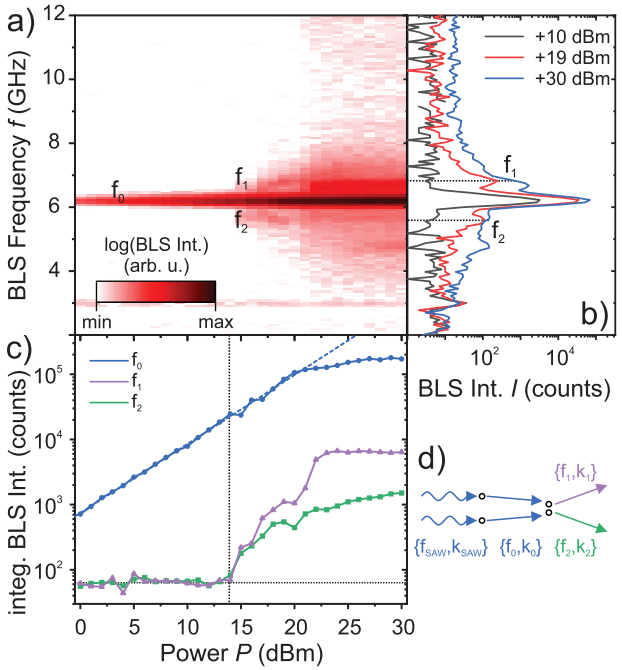

Figure 2. a) Evolution of BLS spectra with the applied RF power and b) exemplary BLS spectra showing linear, critical and supercritical regimes at an external magnetic field of $\mu_0 H_{ext} = 6$mT on a logarithmic intensity scale. c) Logarithmic intensity for directly excited spin waves at $f_0 = 6.3$ GHz (blue) and the intensity of the secondary modes $f_1 = 6.9$ GHz (purple) and $f_2 = 5.7$ GHz (green). A linear progression is indicated by the blue dashed line and the threshold by the vertical black dotted line. d) Schematic illustration of the second order instability process.

Conclusively, we attribute this observation to the following mechanism: Spin waves are resonantly excited by the SAWs, and subsequently undergo a four-magnon scattering process, leading to the second-order spin-wave instability (see Figure 2d). In principle, another four-wave process could be considered, where two SAWs split directly into two spin waves. This process, however, is very unlikely since the Hamiltonian for such a process is described by $\mathcal{H} \sim a_k^2 c_{k_1}^* c_{k_2}^*$, where a_k and c_k are the SAW and spin-wave amplitudes respectively.[53] Usually, the magneto-elastic energy is considered to be a linear function of the strain S, which is

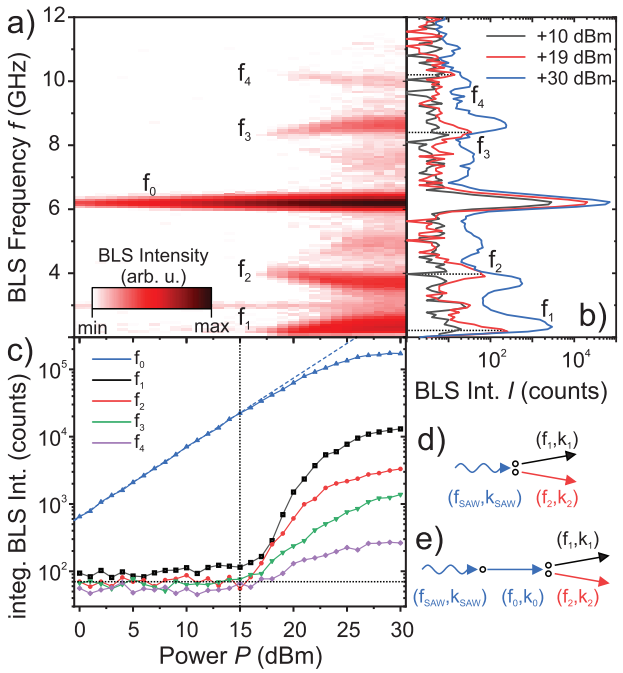

Figure 3. a) Evolution of BLS spectra with the applied RF power a) and exemplary BLS spectra showing linear and critical regimes b) at an external magnetic field of $\mu_0 H_{ext} = 2$mT on a logarithmic intensity scale. c) Logarithmic intensity at $f_0 = 6.3$ GHz (blue) and the intensity of the secondary modes f_1 (red), f_2 (black), f_3 (green) and f_4 (purple). A linear progression is indicated by the blue dashed line and the threshold by the vertical black dotted line.Schematic illustration of d) the acoustic pumping process and e) the non-resonant three-magnon process.

in turn proportional to a_k, so such term in Hamiltonian is absent. Such a process of direct (SAW + SAW)→(SW + SW) instability may only appear at very high SAW amplitudes, not reached in our experiment, at which the linear approximation of the strain ($S_{ij} = 1/2(\partial u_i/\partial x_j + \partial u_j/\partial x_i)$) becomes invalid and/or magnetoelastic coupling becomes strain-dependent.[54]

3.2. Non-Resonant Spin-Wave Excitation and Instability Processes

After considering the case where spin waves are resonantly excited by the SAWs, we will now focus on the non-resonant case. Here, the external magnetic field is reduced to $\mu_0 H_{ext} = 2$mT. As shown in Figure 1b, the spin-wave intensity for the directly excited mode at f_0 is drastically reduced compared to the resonant case. However, instability processes can be observed in this case as shown in **Figure** 3a. In the linear regime, only a signal for the initial mode f_0 is present, which is non-resonantly driven by the SAWs. At high powers, four additional modes with different frequencies f_1 to f_4 are excited and are symmetrically spaced around f_0. Similar to the case of the second-order instability process, it can be stated that all four secondary modes show a common threshold value ($P^{th} = +15$ dBm) within the measurement accuracy (see Figure 3c). These modes are present as dynamical degrees of freedom in the low power regime as well; however, they are not excited at low power.

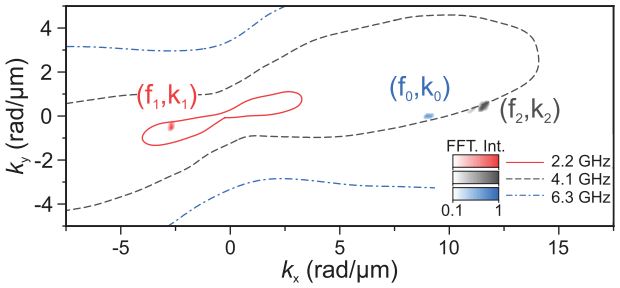

Figure 4. Scheme of first-order instability process. The color patches show the simulated spin-wave intensity while the lines show the isofrequency curves for frequencies f_0 to f_2. The magneto-elastic field is driven with $f_0 = 6.3$ GHz (blue) and leads to pumping of the spin-wave modes $f_1 = 2.2$ GHz (red) and $f_2 = 4.1$ GHz (black) while conserving momentum and energy.

In the following, the origin of the secondary modes f_1 and f_2 will be discussed, while the tertiary modes f_3 and f_4 are addressed in the Supporting Information, since these originate from the interaction between the primary mode and the secondary modes. Near the threshold (see Figure 3b), the secondary modes have frequencies of $f_1 = 2.25$ GHz and $f_2 = 4.05$ GHz, which satisfy the conservation of energy for a three-wave process $f_0 = f_1 + f_2$, i.e., they are equally spaced around half the frequency of the initial mode $f_0/2$. In materials with reciprocal dispersion relation, such frequency nondegenerate splitting, when $f_1 \neq f_2$, is typically observed if the initial mode or correspondingly, the driving field has a non-zero wave vector.

3.3. Micromagnetic Simulations and Theoretical Analysis

In order to determine the wave vectors excited in the observed instability process, micromagnetic simulations were carried out using MuMax3[55] and the software platform Aithericon.[56] The parameters used for the simulations can be found in the Supporting Information.[43] The Rayleigh mode is implemented as a plane wave of the strain components S_{xx} and S_{xz}.[43]

For all simulations a magnetization dynamics with (f_{SAW}, k_{SAW}) = (f_0, k_0) is observed. Once the threshold is exceeded, two secondary spin-wave modes emerge in the simulation: (i) $f_1 = 2.2$ GHz, $\mathbf{k}_1 = (-2.5, -0.5)$ rad/μm and (ii) $f_2 = 4.1$ GHz, $\mathbf{k}_2 = (11.6, 0.5)$ rad/μm (see **Figure** 4). These spin-wave modes preserve, within the accuracy of the simulation, the wave vector of the pumping field, in order to fulfill momentum conservation. In addition, there is a good agreement with the experimentally measured frequencies. The simulated threshold (as well as that theoretically calculated below) corresponds to effective magnetoelastic field $|\mu_0 H_{mel} \approx 1$ mT, while the maximal effective field magnitude (at 30 dBm power) is expected to be $|\mu_0 H_{mel} \sim 10$ mT – high values enough for realization of many nonlinear SW processes.

In Figure 4, the isofrequency curves of the frequencies involved are plotted as lines, which indicate the linear spin-wave eigenmodes at the given frequency. From the simulations, the excited spin wave modes at the frequencies f_0 to f_2 were extracted by means of the Fourier transformation of the magnetization component m_z. While the modes f_1 and f_2 lie on the corresponding isofrequency curves and are thus eigenmodes of the spin-wave

system, this is not the case for the mode f_0. This means that the magneto-elastic field leads to a forced magnetization dynamics with the frequency and wave vector of the SAW (f_{SAW}, k_{SAW}) = (f_0, k_0), which is not an eigenmode of the spin-wave system.

Based on the findings from the experiment and the micromagnetic simulations, two different three-wave processes are conceivable: (i) *acoustic parametric pumping*, which can be understood, in analogy to the parallel pumping of spin waves by electromagnetic waves[57] as the conversion of one phonon into two magnons (see Figure 3d), and (ii) *three-magnon splitting of spin waves*, where in our particular case the excitations at f_0 are forced excitations by the SAW (see Figure 3e). In order to determine which of the two processes is more efficient, the threshold value was theoretically determined for both cases individually. The acoustic pumping of spin waves by SAWs is described by the following rate equation for c_1 and a corresponding equation for c_2:[36]

$$\frac{dc_1}{dt} + i\omega_1 c_1 + \Gamma_1 c_1 = i\,\mathcal{V}_{\mathrm{SAW},12}\, c_2^*\, a_{\mathrm{SAW}}\, e^{-i\omega_{\mathrm{SAW}}t} \tag{1}$$

where c_1 and c_2 are the spin-wave amplitude of the first and second spin-wave mode, Γ_1 the corresponding relaxation rate and a_{SAW} the SAW amplitude. The parametric coupling efficiency consists of two contributions and is given by:

$$\mathcal{V}_{0,12} = \frac{2\gamma B_1}{M_S}\bar{S}_{0,xx}\left(m_{1,x}^* m_{2,x}^* - \mathbf{m}_1^* \cdot \mathbf{m}_2^* \cos^2(\phi_M)\right) \tag{2}$$

Here, $\bar{S}_{0,xx}$ is the thickness average of the SAW strain $S_{0,xx}$, and $\mathbf{m}_\mathbf{k}$ is the spin-wave structure (see details in Supporting Information[43]). The first part of the term within the parentheses, $m_{1,x}^* m_{2,x}^*$, is proportional to the ellipticity of the magnetization trajectory and can be interpreted in analogy to the parametric pumping with electromagnetic waves. The second part, $\mathbf{m}_1^* \cdot \mathbf{m}_2^* \cos^2(\phi_M)$, depends on the dynamic magnetization components m_1 and m_2. This term is characteristic of anisotropy-type pumping, which has been reported for magneto-elastic[36] or magneto-electric[58] drives. The minimal threshold for the acoustic pumping $a_{\mathrm{th,min}}^{\mathrm{SAW-SW}}$ is found for the splitting into magnons with $\mathbf{k}_1$ = (8.1, −0.5)radμm^{-1}, $\mathbf{k}_2$ = (1.2, 0.5) radμm^{-1} and frequencies of [4.2] and 2.1 GHz. The wavevector of these secondary modes differs significantly from those predicted by the micromagnetic simulations.

The second process that needs to be considered is the SAW-driven first order instability, with a forced excitation at (f_{SAW}, $\mathbf{k}_{SAW}$). Just as for the acoustic pumping, a rate equation can be formulated to determine the threshold of this instability. For this purpose, the SAW amplitude a_{SAW} is replaced by the spin-wave amplitude of the non-resonant mode c_0 and the standard three-magnon scattering coefficient $V_{0,12}$[46] is used as the coupling parameter. The link between a_{SAW} and c_0 can be found in the Supporting Information. It turns out that the minimum threshold for this instability process $a_{\mathrm{th,min}}^{\mathrm{3-magnon}}$ is about 64% larger than for the acoustic pumping process. Hence, we conclude that the experimentally observed instability is a combination of the two mentioned three-wave processes. The instability is caused by the acoustic pumping of magnons by SAW phonons. However, even below the threshold of the three-magnon instability $a_{\mathrm{th,min}}^{\mathrm{3-magnon}}$ an energy flow changes the occupation, and thus, the effective damping of the secondary modes. The combination of these two mechanisms results in the threshold values shown in **Figure 5**. The modes with the lowest threshold value for the combined process $a_{\mathrm{th,min}}^{\mathrm{Comb}}$ are marked with stars, the ones for pure acoustic pumping with diamonds and the secondary modes obtained by micromagnetic simulations by squares. The small residual discrepancy between the micromagnetic simulations and the combined process can be attributed to the fact that the threshold varies little in this range (less than 6%). As a result, even small differences in the modeling, for instance in the calculation of the demagnetization field, can explain this small discrepancy between analytical modeling and micromagnetic simulation.

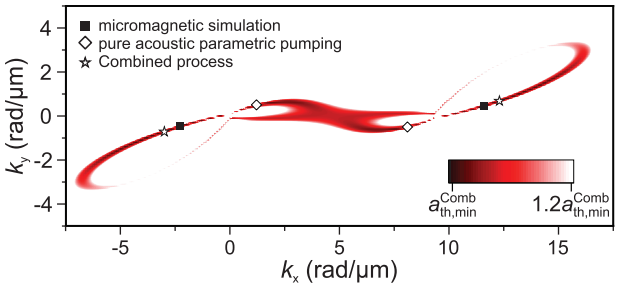

Figure 5. Calculated threshold for the combined process of acoustic pumping influenced by three-magnon scattering. The spin-wave modes with minimal threshold for the direct SAW-SW process $a_{\mathrm{th,min}}^{\mathrm{SAW-SW}}$ (diamond) and the combined process $a_{\mathrm{th,min}}^{\mathrm{Comb}}$ (star) are indicated. The modes extracted from the micromagnetic simulations are shown by the black squares.

4. Conclusion

In summary, in this article we have studied spin-wave instabilities driven by the magneto-elastic field generated by SAWs. We have investigated two different situations. In the resonant case, where spin waves are excited with the wave vector and the frequency of the SAWs, the second-order instability process due to four-magnon scattering process was observed above a certain SAW amplitude threshold. The second case was the non-resonant excitation of the magnetic system by SAWs. Here, we observed a complex combination of scattering processes, which were identified by a combined study of micromagnetic simulations and analytical modeling. The dominant process is the acoustic parametric pumping process of magnons by the SAWs, which is enhanced by three-magnon scattering channels from the forced excitation at the SAW frequency. This contribution of the three-magnon process is crucial for the determination of the secondary modes. It should be emphasized that in contrast to the case of adiabatic parallel pumping, the initial nonzero wave vector of the SAWs leads to a frequency non-degenerate splitting of the secondary modes. This provides an efficient control of the wave vector spectrum of pumped magnons and can be used, e.g., to construct nonlinear frequency converters.[59] Our findings demonstrate that SAW-driven magneto-elastic interaction is sufficiently efficient and large—it allows to reach up to 10 mT effective magnetoelastic field and, thus, observe various nonlinear magnon and magnon-phonon phenomena, which are prerequisites for

magnon information processing systems like phonon-based magnon amplifiers. In combination with well-established low-loss microwave-to-SAW transduction, our work is a step toward efficient nonlinear hybrid magnon-phonon systems.

Supporting Information

Supporting Information is available from the Wiley Online Library or from the author.

Acknowledgements

Financial support by the EU Horizon 2020 research and innovation program within the "CHIRON" project (contract no. 801055) and the European Research Council within the Starting Grant No. 101042439 "CoSpiN" as well as the EU Horizon Europe research and innovation program within the "M&MEMS" project (contract no. 101070536) is gratefully acknowledged. D.N. acknowledges financial support from the Research Foundation -Flanders (FWO) through Grants 1SB9121N. R.V. acknowledges support by the Ministry of Education and Science of Ukraine (project No. 0124U000392).

Conflict of Interest

The authors declare no conflict of interest.

Data Availability Statement

The data that support the findings of this study are available from the corresponding author upon reasonable request.

Keywords

magnetoacoustics, nonlinear interactions, parametric excitation, spin waves, surface acoustic waves (SAWs)

Received: June 14, 2024
Revised: October 1, 2024
Published online: October 19, 2024

[1] A. A. Grachev, O. V. Matveev, M. Mruczkiewicz, M. A. Morozova, E. N. Beginin, S. E. Sheshukova, A. V. Sadovnikov, *Appl. Phys. Lett.* **2021**, *118*, 262405.
[2] A. Bukharaev, A. K. Zvezdin, A. P. Pyatakov, Y. K. Fetisov, *Phys. Usp.* **2018**, *61*, 1175.
[3] Y. K. Fetisov, G. Srinivasan,*Appl. Phys. Lett.* **2006**, *88*, 143503.
[4] A. V. Sadovnikov, A. A. Grachev, S. E. Sheshukova, Y. P. Sharaevskii, A. A. Serdobintsev, D. M. Mitin, S. A. Nikitov, *Phys. Rev. Lett.* **2018**, *120*, 257203.
[5] C. Kittel, *Physical Review* **1958**, *110*, 836.
[6] H. Bömmel, K. Dransfeld, *Phys. Rev. Lett.* **1959**, *3*, 83.
[7] M. Pomerantz, *Phys. Rev. Lett.* **1961**, *7*, 312.
[8] E. Schlömann, *J. Appl. Phys.* **1960**, *31*, 1647.
[9] C. W. Haas, *J. Phys. Chem. Solids* **1966**, *27*, 1687.
[10] H. Matthews, F. R. Morgenthaler, *Phys. Rev. Lett.* **1964**, *13*, 614.
[11] P. Chowdhury, A. Jander, P. Dhagat, *IEEE Magn. Lett.* **2017**, *8*, 1.
[12] N. I. Polzikova, S. G. Alekseev, I. I. Pyataikin, V. A. Luzanov, A. O. Raevskiy, V. A. Kotov, *AIP Adv.* **2018**, *8*, 056128.
[13] S. G. Alekseev, S. E. Dizhur, N. I. Polzikova, V. A. Luzanov, A. O. Raevskiy, A. P. Orlov, V. A. Kotov, S. A. Nikitov, *Appl. Phys. Lett.* **2020**, *117*, 072408.
[14] N. K. P. Babu, A. Trzaskowska, P. Graczyk, G. Centała, S. Mieszczak, H. Głowiński, M. Zdunek, S. Mielcarek, J. W. Kłos, *Nano Lett.* **2021**, *21*, 946.
[15] M. Küß, M. Heigl, L. Flacke, A. Hefele, A. Hörner, M. Weiler, M. Albrecht, A. Wixforth, *Phys. Rev. Appl.* **2021**, *15*, 034046.
[16] W. G. Yang, H. Schmidt, *Appl. Phys. Rev.* **2021**, *8*, 021304.
[17] M. Elhosni, O. Elmazria, S. Petit-Watelot, L. Bouvot, S. Zhgoon, A. Talbi, M. Hehn, K. A. Aissa, S. Hage-Ali, D. Lacour, F. Sarry, O. Boumatar, *Sens. Actuat. A: Phys.* **2016**, *240*, 41.
[18] L. Thevenard, I. S. Camara, S. Majrab, M. Bernard, P. Rovillain, A. Lemaître, C. Gourdon, J.-Y. Duquesne, *Phys. Rev. B* **2016**, *93*, 134430.
[19] M. Xu, K. Yamamoto, J. Puebla, K. Baumgaertl, B. Rana, K. Miura, H. Takahashi, D. Grundler, S. Maekawa, Y. Otani, *Sci. Adv.* **2020**, *6*, eabb1724.
[20] R. Verba, V. Tiberkevich, A. Slavin, *Phys. Rev. Appl.* **2019**, *12*, 054061.
[21] P. J. Shah, D. A. Bas, I. Lisenkov, A. Matyushov, N. X. Sun, M. R. Page, *Sci. Adv.* **2020**, *6*, eabc5648.
[22] P. Delsing, A. N. Cleland, M. J. Schuetz, J. Knörzer, G. Giedke, J. I. Cirac, K. Srinivasan, M. Wu, K. C. Balram, C. Baüerle, T. Meunier, C. J. Ford, P. V. Santos, E. Cerda-Méndez, H. Wang, H. J. Krenner, E. D. Nysten, M. Weiß, G. R. Nash, L. Thevenard, C. Gourdon, P. Rovillain, M. Marangolo, J. Y. Duquesne, G. Fischerauer, W. Ruile, A. Reiner, B. Paschke, D. Denysenko, D. Volkmer, et al.*J. Phys. D: Appl. Phys.* **2019**, *52*, 353001.
[23] C. Caliendo, M. Hamidullah, *J. Phys. D: Appl. Phys.* **2019**, *52*, 153001.
[24] M. Weiler, L. Dreher, C. Heeg, H. Huebl, R. Gross, M. S. Brandt, S. T. B. Goennenwein, *Phys. Rev. Lett.* **2011**, *106*, 117601.
[25] A. Koujok, A. Riveros, D. Rodrigues, G. Finocchio, M. Weiler, A. Hamadeh, P. Pirro, *Appl. Phys. Lett.* **2023**, *123*, 13.
[26] P. J. Shah, D. A. Bas, A. Hamadeh, M. Wolf, A. Franson, M. Newburger, P. Pirro, M. Weiler, M. R. Page, *Adv. Electron. Mater.* **2023**, *9*, 2300524.
[27] P. Kuszewski, J. Y. Duquesne, L. Becerra, A. Lemaître, S. Vincent, S. Majrab, F. Margaillan, C. Gourdon, L. Thevenard, *Phys. Rev. Appl.* **2018**, *10*, 034036.
[28] M. Küß, M. Heigl, L. Flacke, A. Hörner, M. Weiler, M. Albrecht, A. Wixforth, *Phys. Rev. Lett.* **2020**, *125*, 217203.
[29] M. Geilen, A. Nicoloiu, D. Narducci, M. Mohseni, M. Bechberger, M. Ender, F. Ciubotaru, B. Hillebrands, A. Müller, C. Adelmann, P. Pirro, *Appl. Phys. Lett.* **2022**, *120*, 242404.
[30] M. Jaris, W. Yang, C. Berk, H. Schmidt, *Phys. Rev. B* **2020**, *101*, 214421.
[31] F. Godejohann, A. V. Scherbakov, S. M. Kukhtaruk, A. N. Poddubny, D. D. Yaremkevich, M. Wang, A. Nadzeyka, D. R. Yakovlev, A. W. Rushforth, A. V. Akimov, M. Bayer, *Phys. Rev. B* **2020**, *102*, 144438.
[32] J. Janušonis, C. L. Chang, P. H. M. van Loosdrecht, R. I. Tobey, *Appl. Phys. Lett.* **2015**, *106*, 18.
[33] A. Mahmoud, F. Ciubotaru, F. Vanderveken, A. V. Chumak, S. Hamdioui, C. Adelmann, S. Cotofana, *J. Appl. Phys.* **2020**, *128*, 161101.
[34] P. Pirro, V. Vasyuchka, A. A. Serga, B. Hillebrands, *Nat. Rev. Mater.* **2021**, *6*, 227601.
[35] Q. Wang, A. Hamadeh, R. Verba, V. Lomakin, M. Mohseni, B. Hillebrands, A. V. Chumak, P. Pirro, *npj Comput. Mater.* **2020**, *6*, 192.
[36] I. Lisenkov, A. Jander, P. Dhagat, *Phys. Rev. B* **2019**, *99*, 184433.
[37] X. Zhang, G. E. Bauer, T. Yu, *Phys. Rev. Lett.* **2020**, *125*, 077203.
[38] M. Kraimia, P. Kuszewski, J.-Y. Duquesne, A. Lemaître, F. Margaillan, C. Gourdon, L. Thevenard, *Phys. Rev. B* **2020**, *101*, 144425.

[39] C. L. Chang, A. M. Lomonosov, J. Janusonis, V. S. Vlasov, V. V. Temnov, R. I. Tobey, *Phys. Rev. B* **2017**, *95*, 060409.
[40] Á. Papp, W. Porod, G. Csaba, *Nat. Commun.* **2021**, *12*, 6422.
[41] A. A. Hamadeh, D. Slobodianiuk, R. Moukhader, G. Melkov, V. Borynskyi, M. Mohseni, G. Finocchio, V. Lomakin, R. Verba, G. de Loubens, P. Pirro, O. Klein, *Sci. Adv.* **2023**, *9*, eadk1430.
[42] M. Geilen, F. Kohl, A. Nicoloiu, A. Müller, B. Hillebrands, P. Pirro, *Appl. Phys. Lett.* **2020**, *117*, 213501.
[43] Supporting Information.
[44] T. Sebastian, K. Schultheiss, B. Obry, B. Hillebrands, H. Schultheiss, *Front. Phys.* **2015**, *3*, J35.
[45] F. Kargar, A. A. Balandin, *Nat. Photonics* **2021**, *15*, 720.
[46] P. Krivosik, C. E. Patton, *Phys. Rev. B* **2010**, *82*, 184428.
[47] P. Pirro, T. Sebastian, T. Brächer, A. A. Serga, T. Kubota, H. Naganuma, M. Oogane, Y. Ando, B. Hillebrands, *Phys. Rev. Lett.* **2014**, *113*, 227601.
[48] H. Schultheiss, K. Vogt, B. Hillebrands, *Phys. Rev. B* **2012**, *86*, 054414.
[49] A. Gurevich, G. A. Melkov, *Magnetization Oscillations and Waves*, CRC Press, **1996**.
[50] A. Prabhakar, D. D. Stancil, *Spin Waves: Theory and Applications*, Springer New York, NY **2009**.
[51] A. P. Mayer, *Ultrasonics* **2008**, *48*, 478.
[52] A. P. Mayer, *Phys. Rep.* **1995**, *256*, 237.
[53] A. Rückriegel, P. Kopietz, D. A. Bozhko, A. A. Serga, B. Hillebrands, *Phys. Rev. B* **2014**, *89*, 184413.
[54] Z. Tian, D. Sander, J. Kirschner, *Phys. Rev. B* **2009**, *79*, 024432.
[55] A. Vansteenkiste, J. Leliaert, M. Dvornik, M. Helsen, F. Garcia-Sanchez, B. Van Waeyenberge, *AIP Adv.* **2014**, *4*, 107133.
[56] aithericon.com, https://aithericon.com (accessed: July, 2024).
[57] T. Brächer, P. Pirro, B. Hillebrands, *Phys. Rep.* **2017**, *699*, 1.
[58] R. Verba, M. Carpentieri, G. Finocchio, V. Tiberkevich, A. Slavin, *Phys. Rev. Appl.* **2017**, *7*, 064023.
[59] M. Mohseni, A. A. Hamadeh, M. Geilen, P. Pirro, *IEEE Trans. Nanotechnol.* **2023**, *22*, 806.